Assessing the Performance of Density Functional Theory for the Electronic Structure of Metal−Salens: The d^2-Metals

John S. Sears and C. David Sherrill*

Center for Computational Molecular Science and Technology, School of Chemistry and Biochemistry, and College of Computing, Georgia Institute of Technology, Atlanta, Georgia 30332-0400

Received: March 14, 2008; Revised Manuscript Received: April 30, 2008

The performance of three common combinations of density functional theory has been evaluated for the geometries and relative energies of a commonly-employed model complex of the salen ligand [salen = bis(salicylaldehydo)ethylenediamine] with the d^2-metals Ti(II), V(III), Cr(IV), Zr(II), Nb(III), and Mo(IV). High-level ab initio methods including complete active-space third-order perturbation theory have been employed both as benchmarks for the density functional theory results and to examine the multireference character of the low-lying electronic states in these systems. The strong multireference character of the systems has been clearly demonstrated. All of the functionals examined provide geometries that are typically within 0.2 Å least root mean square deviation from the benchmark geometries. The performance of the density functionals for the relative energies of the low-lying electronic states is significantly worse, providing qualitatively different descriptions in some instances. Of the systems explored, no significant difference is observed in the multireference character or in the reliability of the density functional results when comparing 3d vs 4d transition-metal systems.

Introduction

Salen [bis(salicylaldehydo)ethylenediamine] and salen-type ligands currently comprise one of the most important classes of synthetic ligand systems in the context of homogeneous catalysis, where complexes of 3d- and 4d-metals with salen or salen-type ligands have seen numerous applications in asymmetric catalysis.[1–3] With the growing demand for enantiomerically-pure compounds by the pharmaceuticals and fine-chemicals industries, it is not surprising that heterogeneous catalysis via immobilized salen complexes has also been the focus of an extensive amount of research.[3] The design of an appropriate immobilization scheme can be greatly aided by knowledge of the underlying catalytic mechanism, as it has been demonstrated that different immobilization schemes may greatly impact the catalytic activity of immobilized molecular catalysts.[4] Furthermore, the nature of the molecular support may have significant electronic effects upon the immobilized catalysts. Although the development of improved immobilized salen catalysts could be greatly assisted by theoretical insight, theoretical studies of metal−salen catalysts have been somewhat limited. Indeed, with the exception of the Mn(salen) catalysts that have been so extensively studied over the preceding decade,[5–21] few metal−salen systems have seen extensive theoretical investigation. One cause for concern in the theoretical modeling of metal salens is that two of the most common density functional theory (DFT) methods have yielded significant discrepancies when applied to Mn−salen systems.[18] Furthermore, recent work in our group has highlighted the difficulties in applying conventional methods of electronic structure theory to particular metal−salen systems.[22,23]

As pointed out by Davidson in 1991,[24] "The theory of transition-metal chemistry has lagged behind the quantum theory of organic chemistry because quantitative wave functions are more complicated." In particular, the general reliability of DFT methods[25–27] for mixed organic−inorganic systems remains an open question. Although benchmark studies of DFT methods for transition-metal systems exist, these have been limited to metal ions,[28] to transition-metal homo-[29,30] and heterodimers,[31,32] and to systems with a limited number of small ligands.[33–35] Although certainly useful in their own regard, such benchmarks neglect the differing character of the bonding in such systems and of that in the saturated or nearly-saturated metal−ligand systems that are of the most chemical interests (such as in metal−ligand catalyst systems). Furthermore, recent work indicates that systematic errors in popular DFT methods may become increasingly problematic as the size of the system increases.[36]

Although the strong dynamical and nondynamical correlation effects present in metal−ligand systems combined with the difficulties of selecting appropriate references make the application of multireference methods[37–39] extremely challenging for many metal−ligand systems, single-reference formalisms cannot be expected to provide reliable results for such systems. This is not to say, however, that single-reference methods will necessarily fail for metal−ligand systems. The increasingly popular DFT approaches have provided reliable results for many metal−ligand systems,[27,29–31,40–43] although there are certainly many exceptions to this as well.[29–31,43–46] In practice, great care must be taken to ensure that the functional employed provides reliable results for a particular system when DFT is going to be employed for theoretical studies. This can be done either by comparison against reliable experimental data or, in the absence of experimental results, by comparison against results from reliable ab initio calculations. If DFT does indeed provide adequate results, the application of DFT to metal−ligand catalyzed reactions can provide a great deal of chemical insight and understanding.

This work extends to the d^2-metals our previous efforts[22,23] to systematically examine the ability of DFT to describe the electronic structure of metal−salen systems; in particular, we

* Corresponding author. E-mail: sherrill@gatech.edu.

10.1021/jp802249n CCC: $40.75
Published on Web 07/01/2008

consider Ti(II)−, V(III)−, Cr(IV)−, Zr(II)−, Nb(III)−, and Mo(IV)−salens. The geometries and relative energies from DFT are benchmarked against those from high-level ab initio methods capable of accurately treating the multireference nature of the systems. Although the primary purpose of this work is to assess the applicability of DFT to these challenging systems and not to examine in depth the chemical properties of any particular system that has been employed experimentally, several of the metals examined here have been employed previously in metal−salen catalyzed chemical transformations. V(III)−salens have potential application as molecular batteries[47] and have been employed as catalysts in the electroreduction of molecular oxygen.[48–50] Bakac and Guzei have studied hydrogen atom transfer reactions in mixed Cr(IV)/Cr(V)−salen systems.[51] Metal−salen complexes of Zr(II) have been employed as highly efficient and enantioselective catalysts for Baeyer−Villiger oxidation reactions.[52,53] Chiral Nb(III)−salen complexes have recently been employed in asymmetric sulfoxidation reactions[54] with promising results and Mo(IV)−salens have been employed as catalysts in asymmetric olefin epoxidations.[55] The intended goal of the systematic investigation presented here is to provide a detailed examination of the electronic properties and of the performance of DFT for the d^2-metal salens, establishing insight into how both may vary in relation to the formal oxidation state and size of the metal center. It is anticipated that the results presented will inform future applications of DFT to the theoretical investigation of metal−salen catalyzed chemical transformations.

Theoretical Methods

The theoretical approach is similar to that of our previous studies of metal−salen systems.[22,23] All DFT calculations were performed with Jaguar 5.5.[56] The computations were performed using three of the most common combinations of exchange and correlation functionals: the combination of Becke's 1988 exchange functional[57] with Perdew's 1986[58] functional for correlation referred to as BP86, the combination of Becke's 1988 exchange functional with the Perdew−Wang 1991 functional for correlation[59] referred to as BPW91, and the combination of Becke's three-parameter hybrid functional[60] with the correlation functional by Lee, Yang, and Parr[61] referred to as B3LYP. Unless otherwise stated, all DFT calculations employed the pseudospectral implementation of DFT[62] and a fine grid as found in Jaguar 5.5, the Los Alamos basis sets and corresponding effective core potentials of Hay and Wadt (LANL2DZ) for all transition-metal atoms,[63] and a 6-31G* basis for all other atoms.[64] Geometries were completely optimized [root mean square (RMS) gradient 10^{-3} au] for the lowest singlet, triplet, and quintet states using each functional. The nature of the stationary points was verified by computing analytic frequencies.

Geometries were also optimized (RMS gradient 10^{-3} au) at the complete active-space self-consistent field (CASSCF)[38] level with MOLPRO 2006.1.[65] Unless otherwise stated, the converged BP86 geometries were employed as a starting point for these optimizations. Active spaces for CASSCF calculations were chosen by examination of the configuration interaction (CI) vector from large CAS-CI[39] computations performed in a configuration interaction singles and doubles (CISD)[39] natural orbital basis. Starting orbitals for the CASSCF calculations were generated from CASSCF natural orbitals computed in the smaller STO-3G[66–68] basis. The STO-3G CASSCF calculations employed a CISD natural orbital guess. Such an approach has been shown to give reliable convergence for CASSCF calculations on other metal−salen systems, when more conventional approaches have failed to do so.[22] The active spaces and optimized states for each system will be described in the discussion, employing the notation from our previous work.[22] Single-point energy corrections were computed at the CASSCF-optimized geometries at the complete active-space second-order and third-order perturbation theory (CASPT2 and CASPT3) with MOLPRO 2006.1. Due to limitations on the number of correlated orbitals in the CASPT3 program, CASPT3 computations were performed with the lowest σ orbitals frozen and combined as corrections to the internally contracted CASPT2 calculation. All wavefunction-based computations employed a LANL2DZ basis for all second transition-row metals and a 6-31G* basis for all other atoms. All single-point calculations employed the frozen-core approximation using a small-core, defined as 1s2s2p3s and 1s2s2p3s3p3d4s for first and second transition-row metals respectively.

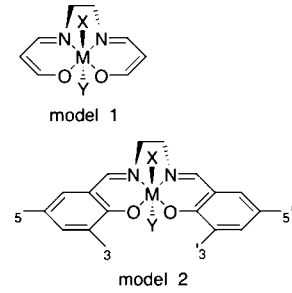

Figure 1. Two of the most common model systems for metal−salen catalysts.

Optimized geometries were compared and the least root mean squared deviations (LRMSD) in molecular geometries were computed using the Visual Molecular Dynamics (VMD) program.[69] Molecular orbital isosurfaces (contour value of 0.05) were generated using MOLEKEL.[70] Information about the multireference nature of the electronic states has been provided by examination of the leading determinants (and coefficients) from the CASSCF CI expansions.

Results and Discussion

Two of the common model systems employed in previous theoretical studies of metal−salen systems are depicted in Figure 1. Although model 2 most nearly delineates the full salen ligand and has been employed in limited studies by previous authors, the truncated model 1 has certainly been the most routinely applied in previous theoretical studies of metal−salen complexes. Given that the truncated model 1 is the most routinely applied in theoretical investigations, this work examines the low-lying electronic states for the systems of the form model 1 [X = none, Y = none, M ∈ {Ti(II), V(III), Cr(IV), Zr(II), Nb(III), Mo(IV)}]. None of the M(salen) complexes studied contain any symmetry elements, and therefore all calculations were performed in C_1 symmetry. The salen ligand does, however, form a pseudo-square-planar coordination sphere around the central metal atom. The definition of appropriate active spaces for the construction of the CASSCF wave functions requires a certain amount of chemical insight, and thus it is useful to consider the important properties of the electronic structure of metal−salen systems before proceeding further. The four coordinating atoms [O, N, N, O] induce a well-known splitting of the metal d-orbital energy levels. Two typical d-orbital splitting diagrams for square-planar coordination presented in the literature are displayed in Figure 2. The degenerate (nearly degenerate for the case of nonsymmetrical coordination) d_{xz} and d_{yz} orbitals are typically considered to be the lowest in energy and this is

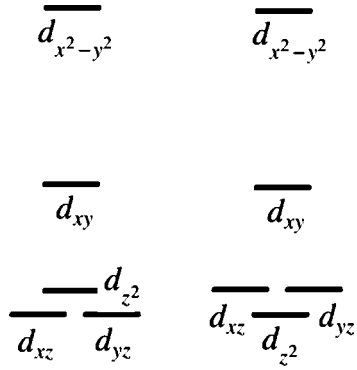

Figure 2. Two commonly presented d-orbital splitting diagrams for a square-planar coordination geometry.

typically true in the weak-field case. The d_{xz} and d_{yz} orbitals are followed closely by the d_{z^2} orbital, and these are energetically well separated from the d_{xy} and the much higher lying $d_{x^2-y^2}$ orbitals. Strong ligand fields, mixing of the s and d_{z^2} orbitals, or strong metal−ligand covalency have been shown to result in a flipping of the ordering of the d_{xz} and d_{yz} orbitals and the d_{z^2} orbital.[71–73] This splitting will play heavily into the construction and interpretation of the active spaces discussed below, as the metal d-orbitals most likely to contribute to the electronic structure will be the low-lying d_{xz}, d_{yz}, and d_{z^2} orbitals. To ascertain the important electronic effects of the salen ligand and further divulge the chemistry taking place in the metal−salen systems, RHF/6-31G* wave functions were constructed (consisting of 55 doubly occupied molecular orbitals) at the BP86 1^1A optimized geometries and the occupied orbitals were localized via Edmiston−Ruedenberg (ER) localization.[74] The anticipated σ bonds occurring in the salen ligand are observed along with the N and O lone pairs involved in dative bonding with the central metal atom. Each O atom has an additional lone pair that is not involved in any bonding interactions. The most important features observed for the electronic structure are the doubly-occupied d_{xz} orbital and the presence of six π-type orbitals on the salen ligand: two representing C−O π bonds, two representing C−N π bonds, and two C−C−C (three-center−two-electron) π bonds hereafter referred to as Rπ_1 and Rπ_2. These are displayed in Figure 3 from the ER localized orbitals of Ti(II)−salen. Given the d^2 electronic configuration (at least in the formal oxidation picture) and the expected near-degeneracies of the metal d-orbitals low-lying singlet and triplet states are anticipated arising from different d-orbital occupations. The quintet states are expected to be higher in energy, arising from mixing of the various d-orbital occupations with either ligand $\pi \rightarrow \pi^*$ excitations or $\pi \rightarrow$ d ligand-to-metal excitations with the latter becoming increasingly important as the formal oxidation state of the metal center is increased. The construction and interpretation of the active spaces for each system and the nature of the low-lying electronic states will be discussed in detail in the following sections.

3d-Metals

Ti(II)−Salen. The relative energies for Ti(II)−salen from the various density functionals in Table 1 reveal the anticipated near-degeneracy of the lowest singlet and triplet states, with the quintet states considerably higher (>60 kcal mol^{-1}) in energy. As has been observed in other metal−salen systems,[22] the hybrid B3LYP overstabilizes the high-spin triplet and quintet states relative to "nonhybrid" functionals (BP86 and BPW91). The relative energies from BP86 and BPW91 are nearly identical

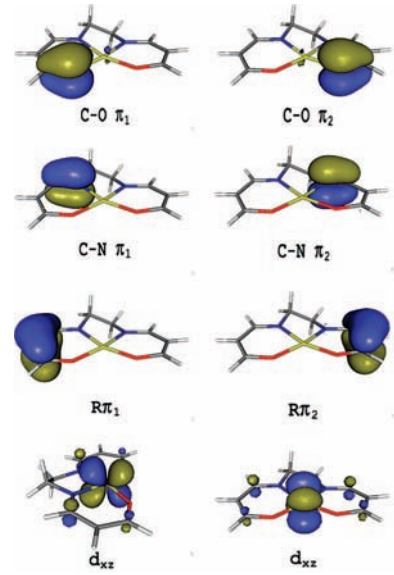

Figure 3. Localized π orbitals of the salen ligand and the localized Ti(II) d_{xz} orbital from a HF/6-31G* calculation of the singlet state of Ti(II)−salen.

TABLE 1: Relative Energies (kcal mol^{-1}) for the Low-Lying Electronic States of Ti(II)−Salen Computed at Various Levels of Theory

	CASPT3	CASPT2	CASSCF	B3LYP	BP86	BPW91
1^1A	13.24	17.76	23.53	10.40	4.27	4.26
2^1A	16.01	18.23	24.24			
3^1A	26.65	23.47	27.94			
1^3A	0.00	0.00	0.00	0.00	0.00	0.00
2^3A	2.23	4.79	3.28			
3^3A	8.18	11.74	9.77			
1^5A				68.67	67.15	66.85

(never differing by more than 0.30 kcal mol^{-1}). This is consistent with previous observations that the spin-state splittings are dominated by the exchange treatment.[22,23] CAS-CI computations including up to 14 electrons in 13 orbitals reveal a similar picture of nearly degenerate singlet and triplet states with a much higher-lying quintet state. The three lowest singlet and triplet states appear energetically well separated from remaining electronic states and have been optimized at the SA-CASSCF(2/3)/6-31G*[1^1A,2^1A,3^1A,1^3A,2^3A,3^3A] level of theory, where (SA-) indicates that the CASSCF optimizations were preformed with state averaging over the relevant electronic states and the states in brackets are those included in the state averaging. All of the states appear to be well described by an active space consisting of two electrons in the three lowest-lying (d_{z^2}, d_{xz}, and d_{yz}) d-orbitals. The active space is depicted in Figure 4 from the SA-CASSCF optimization of the 1^1A state and the relative energies for all states are included in Table 1. The CASSCF results reveal three triplet states below 10 kcal mol^{-1} followed by three low-lying singlet states below 30 kcal mol^{-1}. The inclusion of dynamical correlation reduces the splitting of the lowest singlet and triplet states (23.53 kcal mol^{-1} at the SA-CASSCF level) to 17.76 kcal mol^{-1} at the CASPT2 level and 13.24 kcal mol^{-1} at the CASPT3 level. This is coherent with previous observations that corrections for dynamical electron correlation tend to stabilize low-spin electronic states. Overall, a consistent picture of the lowest singlet and triplet states of Ti(II)−salen is provided by all methods.

The optimized geometries of the 1^1A and 1^3A state from DFT and CASSCF are overlaid in Figure 5. The geometries from all

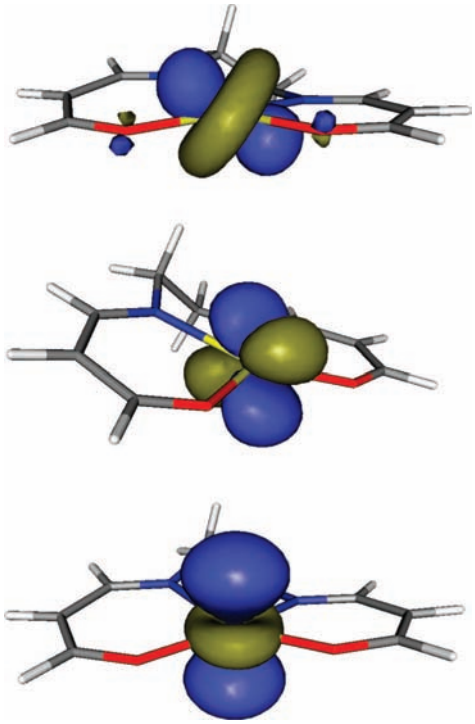

Figure 4. Isosurface plots of the d_{z^2} (lower), d_{xz} (center), and d_{yz} (upper) CASSCF orbitals that comprise the active space for Ti(II)−salen.

methods are visibly very similar and this is confirmed by the LRMSD values included in Table 2. The DFT geometries never differ by more than 0.035 Å and are all within 0.2 Å LRMSD of the CASSCF optimized geometries. In consensus with previous results,[23] the geometries from BP86 and BPW91 are nearly indistinguishable. B3LYP provides geometries that are overall closer to the CASSCF geometries, although marginally so.

The multireference character of the low-lying electronic states has been explored by examination of the leading determinants from the SA-CASSCF computations. The determinants and coefficients for Ti(II)−salen (included in Table 3) reveal the strong multireference nature of the states examined. The ground state is dominated by the anticipated $(d_{z^2})\alpha(d_{xz})\alpha$ electronic configuration, but with a surprisingly small leading coefficient of 0.827 and a very large contribution (0.562) from the $(d_{xz})\alpha(d_{yz})\alpha$ configuration. With the exception of the 1^1A state, all of the states investigated exhibit even stronger nondynamical effects (smaller leading coefficients) than the 1^3A ground state. Even for the 1^1A state, the leading coefficient (0.905) is significantly smaller than would be expected for well-behaved single-reference systems. The low-lying singlet states are dominated by the closed-shell $(d_{z^2})^2$ and $(d_{xz})^2$ configurations with surprisingly little contribution from the complementary $(d_{yz})^2$ configuration. Despite the large nondynamical effects present in Ti(II)−salen, the DFT approaches provide very reasonable agreement with our best results. For this case, B3LYP geometries are closer to those from CASSCF (LRMSD < 0.159 Å), and relative energies in very good agreement with CASPT3 results (ΔE_{rel} < 2.84 kcal mol^{-1}).

V(III)−Salen. CAS-CI computations for V(III)−salen reveal an electronic structure very similar to that for the isoelectronic Ti(II)−salen presented above. The three lowest singlet and triplet states were optimized at the SA-CASSCF(2/3)/6-31G*[1^1A,2^1A,3^1A,1^3A,2^3A,3^3A] level of theory employing the active space depicted in Figure 6 from the SA-CASSCF optimization of the 1^3A state. The relative energies for these

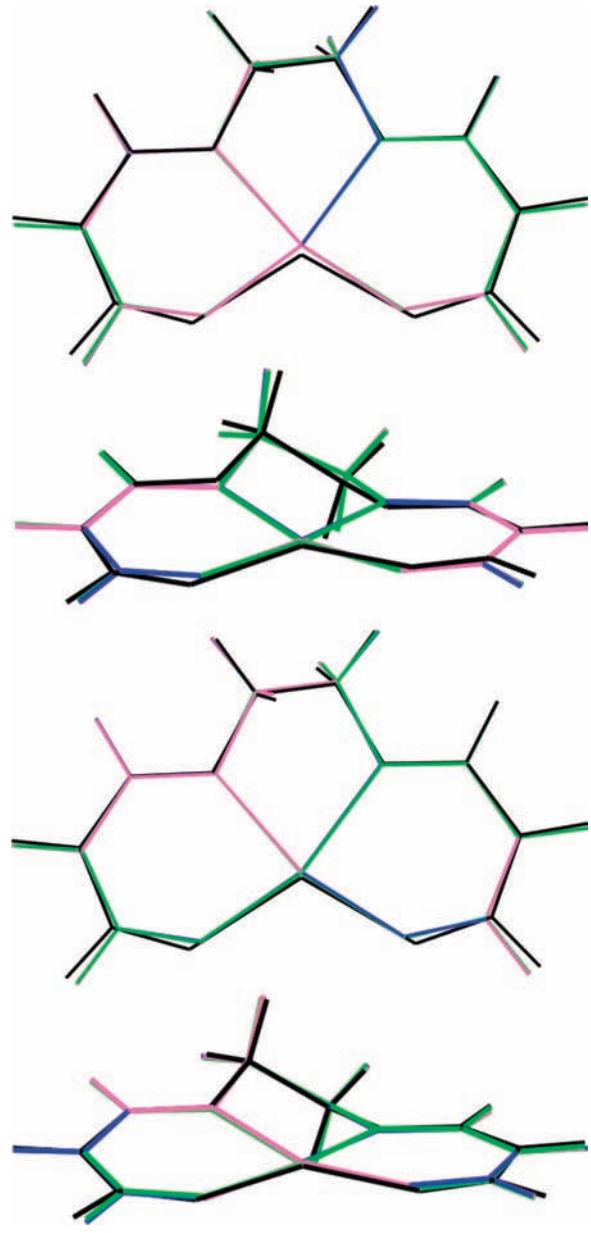

Figure 5. Overlay of the optimized geometries for the 1^1A (top) and 1^3A (bottom) states of Ti(II)−salen from different levels of theory. The theoretical methods include CASSCF (black), B3LYP (green), BP86 (blue), and BPW91 (mauve).

TABLE 2: LRMSD(Å) in Molecular Geometries for the 1^1A and 1^3A States of (Lower Triangular) Ti(II)− and (Upper Triangular) Zr(II)−Salens

		CASSCF	B3LYP	BP86	BPW91		
Ti(II)	CASSCF		0.129	0.147	0.143	CASSCF	Zr(II)
		0.133	0.141	0.138			
	B3LYP	0.159		0.029	0.025	B3LYP	
	0.100		0.017	0.015			
	BP86	0.175	0.021		0.011	BP86	
	0.116	0.035		0.004			
	BPW91	0.173	0.019	0.003		BPW91	
	0.112	0.035	0.005				

states from all multireference computations along with the relative energies from DFT for the 1^{1A}, 1^3A, and 1^5A states are included in Table 4. The CASPT3 results predict the anticipated ^{3}A ground state for the system. The singlet state is predicted to lie slightly more than 20 kcal mol^{-1} higher in energy, a value that is remarkably well matched by the B3LYP results.

TABLE 3: Leading Determinants from SA-CASSCF Calculations on the Low-Lying Electronic States of Ti(II)−Salen

state	determinant	coefficient
1^1A	$(d_{z^2})^2$	0.9050
	$(d_{xz})^2$	−0.4094
2^1A	$(d_{z^2})^2$	0.7071
	$(d_{yz})^2$	−0.7071
3^1A	$(d_{z^2})\alpha(d_{yz})\beta$	0.6022
	$(d_{z^2})\beta(d_{yz})\alpha$	−0.6022
	$(d_{xz})^2$	0.4917
	$(d_{yz})^2$	−0.1752
1^3A	$(d_{z^2})\alpha(d_{xz})\alpha$	0.8272
	$(d_{xz})\alpha\ (d_{yz})\alpha$	0.5619
2^3A	$(d_{z^2})\alpha(d_{yz})\alpha$	0.6811
	$(d_{xz})\alpha(d_{yz})\alpha$	0.6784
	$(d_{z^2})\alpha(d_{xz})\alpha$	−0.2753
3^3A	$(d_{xz})\alpha(d_{yz})\alpha$	0.7077
	$(d_{z^2})\alpha(d_{yz})\alpha$	−0.7066

TABLE 4: Relative Energies (kcal mol^{-1}) for the Low-Lying Electronic States of V(III)−Salen Computed at Various Levels of Theory

	CASPT3	CASPT2	CASSCF	B3LYP	BP86	BPW91
1^1A	20.71	23.56	30.71	20.29	14.48	14.85
2^1A	20.74	23.06	31.03			
3^1A	26.28	28.50	35.84			
1^3A	0.85	0.00	0.00	0.00	0.00	0.00
2^3A	0.00	0.44	1.02			
3^3A	5.53	7.95	9.24			
1^5A				35.34	39.23	38.29

Interestingly, the 1^3A and 2^3A states [split by approximately 2 kcal mol^{-1} in Ti(II)−salen] are nearly degenerate in V(III)−salen with the CASPT3 results flipping the state ordering relative to the CASPT2 and CASSCF results. The states are labeled with respect to the ordering observed in the SA-CASSCF computations. All multireference approaches place the 1^3A and 2^3A states within 1 kcal mol^{-1} of each other, which is within the anticipated error bars for the results. A similar effect is observed for the 1^1A and 2^1A states as well, being separated by only 0.03 kcal mol^{-1} at the CASPT3 level of theory. Again, corrections for dynamical electron correlation tend to stabilize the 1^1A state relative to the 1^3A state. Although BP86 and BPW91 predict the correct ordering of the electronic states, both functionals predict the 1^1A state to be more stable than that observed in our most reliable results. Overall, B3LYP provides superior agreement with CASPT3 for the relative energies in V(III)−salen.

The optimized geometries of the 1^1A and 1^3A states of V(III)−salen are overlaid in Figure 7. The DFT geometries for both states are nearly indistinguishable, in both cases being more planar than the corresponding CASSCF geometry. Overall, the differences between the DFT and CASSCF geometries are slightly larger than those observed in Ti(II)−salen. The LRMSDs presented in Table 5 reveal the B3LYP geometries to be somewhat closer to the CASSCF geometries than are those from BP86 or BPW91, although the difference is clearly negligible. All of the functionals examined perform similarly in comparison to CASSCF for the geometries of both the 1^1A and 1^3A states.

The leading determinants from the SA-CASSCF computations are presented in Table 6. The 1^1A and 2^1A states are demonstrated to be qualitatively similar to the corresponding states in Ti(II)−salen, with somewhat increased multireference character. Relative to Ti(II)−salen, the weight of the leading determinant is smaller and the weight of the second determinant is larger for both states. This is in contrast to the low-lying triplet states,

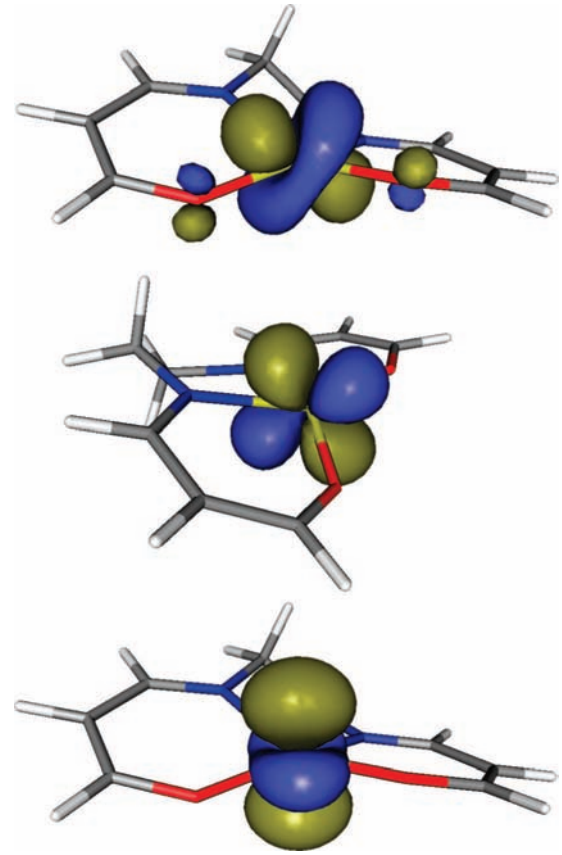

Figure 6. Isosurface plots of the d_{z^2} (lower), d_{xz} (center), and d_{yz} (upper) CASSCF orbitals that comprise the active space for V(III)−salen.

which become increasingly single-reference with the increased oxidation state. The leading coefficients (0.969, 1.000, and 1.000—note the use of a small active space) are closer to what would be expected for well-behaved single-reference systems. Being very similar to Ti(II)−salen, B3LYP provides geometries and relative energies that are closer to our best results than are the BP86 and BPW91 results (LRMSD < 0.200 Å, ΔE_{rel} < 0.42 kcal mol^{-1}).

Cr(IV)−Salen. The increased formal oxidation state in Cr(IV) leads to strong mixing of the metal d-orbitals with the Rπ orbitals of the salen ligand, providing an electronic structure distinctly different from that observed in Ti(II)− and V(III)−salen above. CAS-CI computations for Cr(IV)−salen reveal the strong mixing of the metal and ligand orbitals as well as the increased nondynamical correlation effects which result. The three low-lying singlet and triplet states observed in the previous systems are significantly split as a consequence, giving rise to a low-lying singlet and a low-lying triplet state. The computations further demonstrate the existence of two nearly-degenerate low-lying quintet states. These states were optimized at the SA-CASSCF(6/6)/6-31G*[1^1A,1^3A,1^5A,2^5A] level of theory with an active space consisting of the ligand Rπ orbitals and the four lowest-lying Cr d-orbitals. These are depicted in Figure 8 from the SA-CASSCF computation of the 1^3A state. The SA-CASSCF orbitals clearly reveal the strong mixing of the ligand Rπ and Cr d_{xz} and d_{yz} orbitals. The orbitals have been labeled in the figure based upon the dominant d-orbital character. The multireference results reveal nearly degenerate 1^3A, 1^{5A}, and 2^5A states with small corrections to the relative energies for dynamical electron correlation. It should be noted that the presence of intruder states required the use of a level shift (0.3) in the CASPT2 computations.

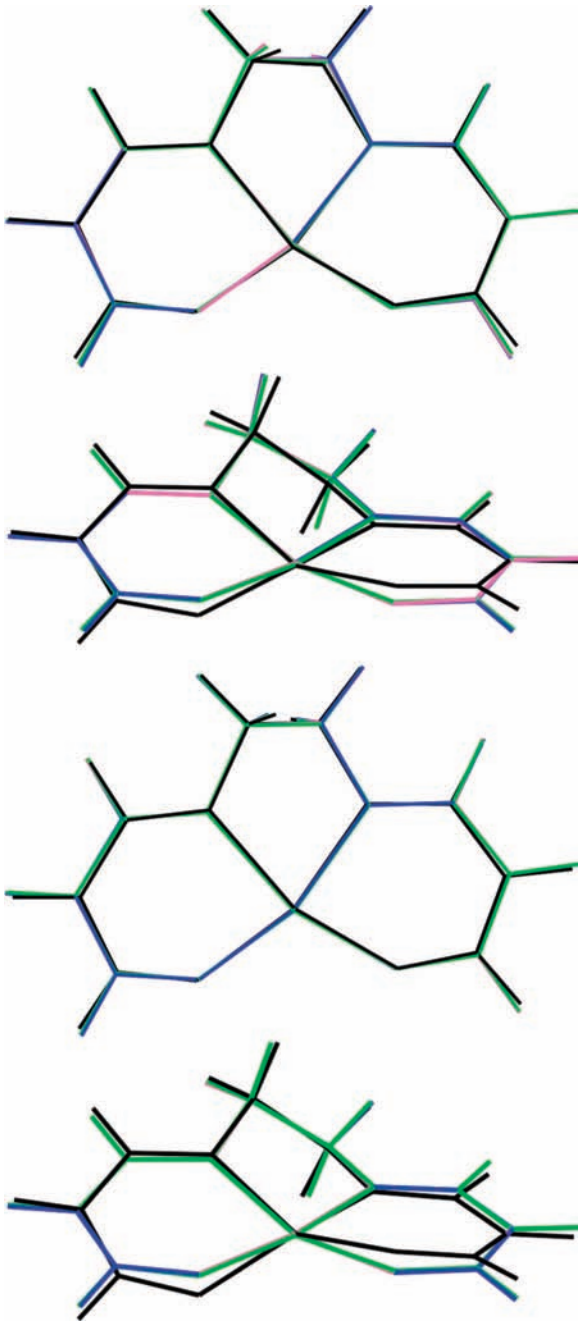

Figure 7. Overlay of the optimized geometries for the 1^1A (top) and 1^3A (bottom) states of V(III)−salen from different levels of theory. The theoretical methods include CASSCF (black), B3LYP (green), BP86 (blue), and BPW91 (mauve).

TABLE 5: LRMSD(Å) in Molecular Geometries for the 1^1A and 1^3A States of (Lower Traingular) V(III)− and (Upper Triangular) Nb(III)−Salens

		CASSCF	B3LYP	BP86	BPW91		
V(III)	CASSCF		0.326	0.399	0.401	CASSCF	Nb(III)
			0.441	0.067	0.064		
	B3LYP	0.194		0.093	0.085	B3LYP	
		0.200		0.454	0.457		
	BP86	0.216	0.034		0.021	BP86	
		0.209	0.019		0.007		
	BPW91	0.211	0.028	0.008		BPW91	
		0.207	0.015	0.006			

That the electronic structure of Cr(IV)−salen is dissimilar from the previous systems is obvious from the relative energies predicted by DFT. The DFT approaches provide qualitatively different descriptions of the electronic state ordering for this system, as can be observed from the relative energies in Table 7. All functionals predict the 1^5A state to be significantly lower in energy than in the previous systems, with B3LYP predicting a 1^5A ground state. BP86 and BPW91 again provide a very similar description of the electronic state ordering, with relative energies differing by no more than 1.71 kcal mol^{-1}. Unlike in the Ti(II)− and V(III)−salen systems presented above, the BP86 and BPW91 functionals provide relative energies somewhat closer to our best results than those from B3LYP. However, the performance of all functionals is markedly worse for the relative energies of Cr(IV)−salen than for the other $3d^2$-metal salens presented above. Although strong mixing of the Rπ orbitals with the Cr d_{xz} and d_{yz} orbitals is clearly evident from Figure 8, the resulting CI coefficients (included in Table 8)

TABLE 6: Leading Determinants from SA-CASSCF Calculations on the Low-Lying Electronic States of V(III)−Salen

state	determinant	coefficient
1^1A	$(d_{z^2})^2$	0.8737
	$(d_{xz})^2$	−0.4697
2^1A	$(d_{z^2})^2$	0.7070
	$(d_{yz})^2$	−0.7070
3^1A	$(d_{xz})^2$	0.7392
	$(d_{yz})^2$	−0.4777
	$(d_{z^2})\alpha(d_{yz})\beta$	0.3020
	$(d_{z^2})\beta(d_{yz})\alpha$	−0.3020
	$(d_{z^2})^2$	0.2071
1^3A	$(d_{xz})\alpha(d_{yz})\alpha$	0.9694
	$(d_{z^2})\alpha(d_{xz})\alpha$	0.2455
2^3A	$(d_{z^2})\alpha(d_{yz})\alpha$	1.0000
3^3A	$(d_{z^2})\alpha(d_{xz})\alpha$	1.0000

TABLE 7: Relative Energies (kcal mol^{-1}) for the Low-Lying Electronic States of Cr(IV)−Salen Computed at Various Levels of Theory

	CASPT3	CASPT2	CASSCF	B3LYP	BP86	BPW91
1^1A	55.14	55.85	60.25	24.71	19.34	19.87
1^3A	0.00	0.00	0.00	4.31	0.00	0.00
1^5A	8.48	0.19	0.61	0.00	11.52	9.81
2^5A	13.51	1.11	0.88			

TABLE 8: Leading Determinants from CASSCF Calculations on the Low-Lying Electronic States of Cr(IV)−Salen

state	determinant	coefficient
1^1A	$(R\pi_1)^2(R\pi_2)\alpha(d_{xz})\beta(d_{yz})\beta(d_{x^2-y^2})\alpha$	0.3109
	$(R\pi_1)^2(R\pi_2)\beta(d_{xz})\alpha(d_{yz})\alpha(d_{x^2-y^2})\beta$	0.3109
	$(d_{z^2})^2(R\pi_2)\beta(d_{xz})\alpha(d_{yz})\alpha(d_{x^2-y^2})\beta$	−0.2430
	$(d_{z^2})^2(R\pi_2)\alpha(d_{xz})\beta(d_{yz})\beta(d_{x^2-y^2})\alpha$	−0.2430
	$(R\pi_1)^2(R\pi_2)^2(d_{xz})^2$	−0.2257
	$(R\pi_1)^2(R\pi_2)^2(d_{x^2-y^2})^2$	0.2135
1^3A	$(R\pi_1)^2(R\pi_2)^2(d_{yz})\alpha(d_{xz})\alpha$	−0.3498
	$(R\pi_1)^2(d_{x^2}\text{-}y^2)^2(d_{yz})\alpha(d_{xz})\alpha$	0.3346
	$(R\pi_1)^2(d_{z^2})^2(d_{yz})\alpha(d_{xz})\alpha$	0.2781
	$(R\pi_1)^2(R\pi_2)\beta(d_{xz})\alpha(d_{yz})\alpha(d_{x^2-y^2})\alpha$	0.2737
	$(d_{x^2-y^2})^2(d_{z^2})^2(d_{yz})\alpha(d_{xz})\alpha$	−0.2701
	$(d_{z^2})^2(R\pi_2)\beta(d_{xz})\alpha(d_{yz})\alpha(d_{x^2-y^2})\alpha$	−0.2190
1^5A	$(R\pi_1)^2(R\pi_2)\alpha(d_{yz})\alpha(d_{xz})\alpha(d_{x^2-y^2})\alpha$	0.4885
	$(R\pi_2)^2(d_{xz})\alpha(R\pi_1)\alpha(d_{yz})\alpha(d_{z^2})\alpha$	−0.4142
	$(d_{x^2-y^2})^2(R\pi_1)\alpha(R\pi_2)\alpha(d_{yz})\alpha(d_{z^2})\alpha$	0.3996
	$(d_{z^2})^2(R\pi_2)\alpha(d_{xz})\alpha(d_{yz})\alpha(d_{x^2-y^2})\alpha$	−0.3920
	$(R\pi_1)\alpha(d_{yz})\beta(R\pi_2)\alpha(d_{xz})\alpha(d_{x^2-y^2})\alpha(d_{z^2})\alpha$	−0.2788
	$(R\pi_2)\alpha(d_{xz})\beta(R\pi_1)\alpha(d_{yz})\alpha(d_{x^2-y^2})\alpha(d_{z^2})\alpha$	−0.2759
	$(d_{xz})\alpha(R\pi_2)\beta(R\pi_1)\alpha(d_{yz})\alpha(d_{x^2-y^2})\alpha(d_{z^2})\alpha$	0.2581
2^5A	$(R\pi_2)^2(d_{xz})\alpha(R\pi_1)\alpha(d_{yz})\alpha(d_{x^2-y^2})\alpha$	0.4377
	$(R\pi_1)^2(d_{yz})\alpha(d_{xz})\alpha(d_{x^2-y^2})\alpha(d_{z^2})\alpha$	−0.4004
	$(d_{z^2})^2(R\pi_1)\alpha(d_{yz})\alpha(d_{xz})\alpha(d_{x^2-y^2})\alpha$	−0.3757

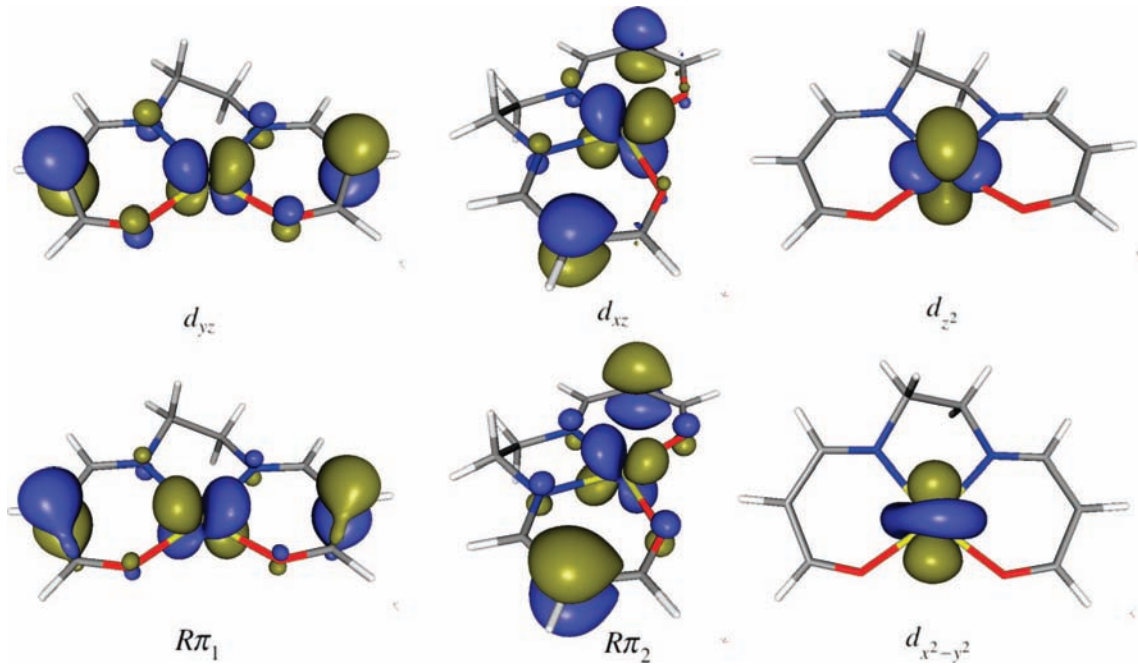

Figure 8. Isosurface plots of the orbitals comprising the active space for Cr(IV)−Salen.

TABLE 9: LRMSD (Å) in Molecular Geometries for the 1^1A, 1^{3A}, and 1^5A States of (Lower Triangular) Cr(IV)− and (Upper Triangular) Mo(IV)−Salens

		CASSCF	B3LYP	BP86	BPW91		
	CASSCF		0.150	0.160	0.160	CASSCF	
			0.084	0.097	0.093		
	B3LYP	0.131		0.026	0.023	B3LYP	
		0.140		0.016	0.016		
Cr(IV)		0.174					Mo(IV)
	BP86	0.140	0.025		0.006	BP86	
		0.134	0.023		0.005		
		0.198	0.034				
	BPW91	0.137	0.020	0.006		BPW91	
		0.133	0.017	0.008			
		0.183	0.030	0.018			

TABLE 10: Relative Energies (kcal mol^{-1}) for the Low-Lying Electronic States of Zr(II)−Salen Computed at Various Levels of Theory

	CASPT3	CASPT2	CASSCF	B3LYP	BP86	BPW91
1^1A	9.69	13.59	15.00	9.69	6.48	6.32
2^1A	16.13	17.67	18.70			
3^1A	32.65	33.24	28.79			
1^3A	0.00	0.00	0.00	0.00	0.00	0.00
2^3A	23.43	26.58	15.52			
3^3A	38.54	41.47	25.44			
1^5A				68.51	66.45	66.26

reveal the extremely strong multireference character of the electronic states. The leading coefficients are never larger than 0.4885 for all of the states explored. It should be noted that the use of natural orbitals from the SA-CASSCF density matrix (as opposed to "state specific" natural orbitals), although providing for a consistent set of molecular orbitals for describing the electronic structure of all states, could serve to enhance both the mixing of the active-space orbitals as well as the number of important electronic configurations. Such effects are anticipated to be moderate and do not detract from the comparison of the geometries and relative energies to those from the DFT approaches. Surprisingly, the DFT approaches provide geometries closer to the CASSCF geometries than was observed for Ti(II)− or V(III)−salen. This can be clearly seen from Figure 9 and from the LRMSD values in Table 9. Although B3LYP provides geometries that are somewhat closer to CASSCF than are those from BP86 and BPW91, all of the functionals provide similar agreement for the geometries of Cr(IV)−salen.

TABLE 11: Leading Determinants from SA-CASSCF Calculations on the Low-Lying Electronic States of Zr(II)−Salen

state	determinant	coefficient
1^1A	$(d_{z^2})^2$	0.9093
	$(d_{xz})^2$	−0.4077
2^1A	$(d_{z^2})^2$	0.7071
	$(d_{yz})^2$	−0.7071
3^1A	$(d_{z^2})^2$	0.778
	$(d_{xz})^2$	−0.544
	$(d_{yz})^2$	−0.210
1^3A	$(d_{z^2})\alpha(d_{xz})\alpha$	0.9922
2^3A	$(d_{z^2})\alpha(d_{yz})\alpha$	1.0000
3^3A	$(d_{xz})\alpha(d_{yz})\alpha$	0.9874
	$(d_{z^2})\alpha(d_{yz})\alpha$	0.1580

4d-Metals

Zr(II)−Salen. CAS-CI computations on Zr(II)−salen reveal a similar electronic structure to that of Ti(II)−salen presented above. The relative energies computed at the SA-CASSCF(2/3)/6-31G*[1^1A,2^1A,3^1A,1^3A,2^3A,3^3A] level are included in Table 10 and compared to those from DFT. The active-space orbitals form the SA-CASSCF optimization of the 1^1A state are depicted in Figure 10. It is generally assumed that complexes of 4d metals exhibit smaller nondynamical correlation effects and larger electronic state splittings.[75] However, the splitting of the lowest singlet and triplet states is apparently slightly smaller for Zr(II)−salen than for Ti(II)−salen (9.69 vs 13.24 kcal mol^{-1} using CASPT3). Somewhat surprisingly, the singlet−triplet splitting from B3LYP is identical to the CASPT3 result. The nonhybrid, generalized gradient approaches (BP86 and BPW91) slightly underestimate the stability of the triplet state compared to the B3LYP and the high-level CASPT3 results.

The overlays of the optimized 1^1A and 1^3A geometries are displayed in Figure 11. Again, the geometries provided by all

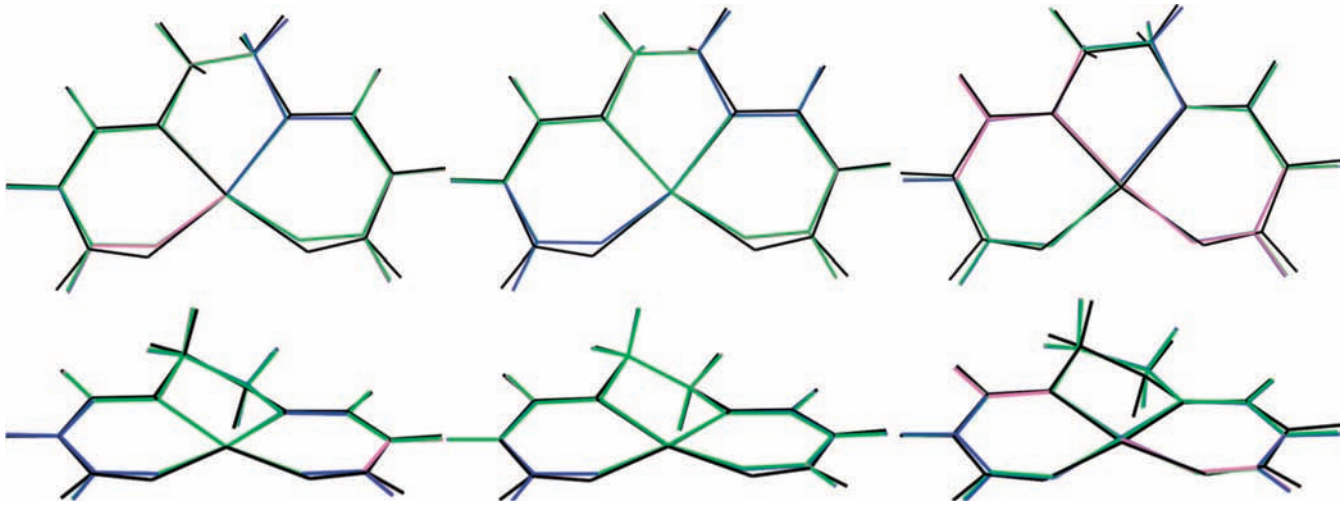

Figure 9. Overlay of the optimized geometries for the 1^1A (left), 1^3A (center), and 1^5A (right) states of Cr(IV)−salen from different levels of theory. The theoretical methods include CASSCF (black), B3LYP (green), BP86 (blue), and BPW91 (mauve).

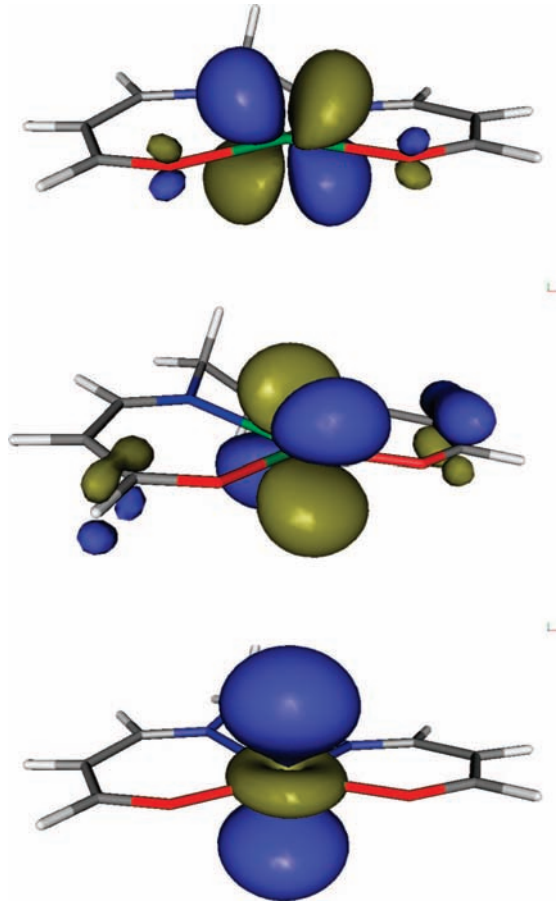

Figure 10. Isosurface plots of the d_{z^2} (lower), d_{xz} (center), and d_{yz} (upper) CASSCF orbitals that comprise the active space for Zr(II)−salen.

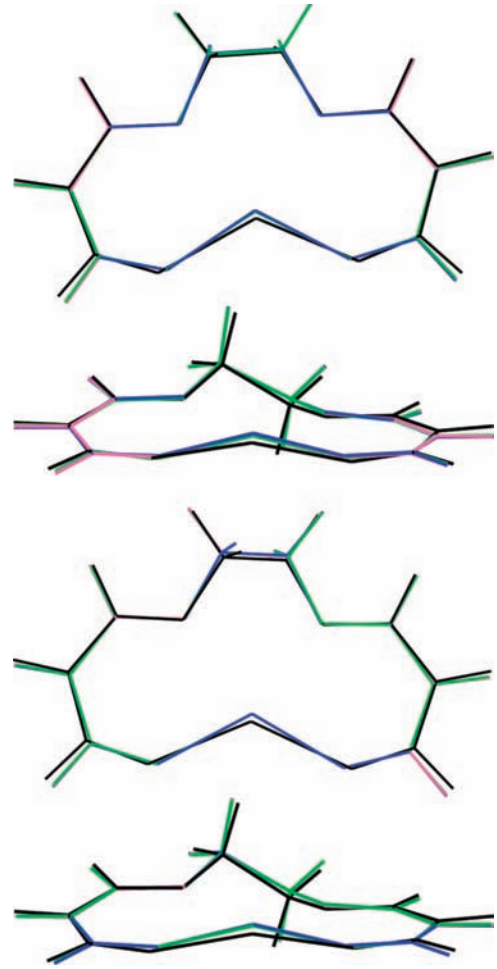

Figure 11. Overlay of the optimized geometries for the 1^1A (top) and 1^3A (bottom) states of Zr(II)−salen from different levels of theory. The theoretical methods include CASSCF (black), B3LYP (green), BP86 (blue), and BPW91 (mauve).

functionals agree very well with those from CASSCF. The comparison is similar to that witnessed in Ti(II)−salen, as is evident from the LRMSD values in Table 2. As has been observed previously in other metal−salen systems,[23] DFT predicts a slightly larger out-of-plane puckering of the central metal atom when compared to the CASSCF results.

The leading determinants from the SA-CASSCF computation are presented in Table 11. The triplet state are all predicted to be strongly single-reference (leading coefficients of 0.999, 1.000, and 0.987 respectively). In contrast, the singlet states remain strongly multireference and the coefficients are very similar to those observed in Ti(II)−salen above.

Nb(III)−Salen. The relative energies from all methods for the low-lying electronic states of Nb(III)−salen are included in Table 12. CAS-CI computations reveal a very similar electronic structure to Zr(II)−salen above, with three low-lying singlet and triplet states well described by the same 2-in-3 active

TABLE 12: Relative Energies (kcal mol^{-1}) for the Low-Lying Electronic States of Nb(III)−Salen Computed at Various Levels of Theory

	CASPT3	CASPT2	CASSCF	B3LYP	BP86	BPW91
1^1A	19.78	19.57	18.30	1.39	13.37	14.00
2^1A	20.71	20.83	18.99			
3^1A	29.42	29.50	29.77			
1^3A	0.00	0.00	0.00	0.00	0.00	0.00
2^3A	12.75	13.21	9.62			
3^3A	25.45	23.63	13.11			
1^5A				47.09	57.81	57.07

TABLE 13: Leading Determinants from SA-CASSCF Calculations on the Low-Lying Electronic States of Nb(III)−Salen

state	determinant	coefficient
1^1A	$(d_{z^2})^2$	0.8083
	$(d_{xz})^2$	−0.5855
2^1A	$(d_{z^2})\alpha(d_{xz})\beta$	0.7070
	$(d_{z^2})\beta(d_{xz})\alpha$	−0.7070
3^1A	$(d_{xz})^2$	0.7633
	$(d_{z^2})^2$	0.4340
	$(d_{yz})^2$	−0.4034
	$(d_{z^2})\beta(d_{yz})\alpha$	0.1821
	$(d_{z^2})\alpha(d_{yz})\beta$	−0.1821
	$(d_{z^2})\alpha(d_{yz})\beta$	−0.1821
1^3A	$(^d_{z^2})\alpha(d_{xz})\alpha$	0.9960
2^3A	$(^d_{z^2})\alpha(d_{yz})\alpha$	0.9882
3^3A	$(^d_{xz})\alpha(d_{yz})\alpha$	0.9957

TABLE 14: Relative Energies (kcal mol^{-1}) for the Low-Lying Electronic States of Mo(IV)−Salen Computed at Various Levels of Theory

	CASPT3	CASPT2	CASSCF	B3LYP	BP86	BPW91
1^1A	23.21	21.98	19.26	16.47	14.75	14.96
2^1A	22.34	22.80	19.40			
3^1A	31.34	30.50	32.72			
1^3A	0.00	0.00	0.00	0.00	0.00	0.00
2^3A	7.52	7.99	1.91			
3^3A	33.84	35.58	32.72			
1^5A				26.12	32.01	31.08

TABLE 15: Leading Determinants from SA-CASSCF Calculations on the Low-Lying Electronic States of Mo(IV)−Salen

state	determinant	coefficient
1^1A	$(d_{z^2})^2$	0.7622
	$(d_{xz})^2$	−0.6459
2^1A	$(d_{z^2})\alpha(d_{xz})\beta$	0.7071
	$(d_{z^2})\beta(d_{xz})\alpha$	−0.7071
3^1A	$(d_{xz})^2$	0.7601
	$(d_{z^2})^2$	0.5542
	$(d_{yz})^2$	−0.3182
1^3A	$(d_{z^2})\alpha(d_{xz})\alpha$	0.9982
2^3A	$(d_{z^2})\alpha(d_{yz})\alpha$	1.0000
3^3A	$(d_{xz})\alpha(d_{yz})\alpha$	0.9982

space (depicted in Figure 12). With the exception of the 3^3A state, the SA-CASSCF(2/3)/6-31G*[1^1A,2^1A,3^1A,1^3A,2^3A,3^3A] relative energies are not changed by much upon correction for dynamical correlation via CASPT2 and CASPT3. From the leading coefficients (Table 13), all of the singlet states are observed to be strongly multireference. Although the open-shell 2^1A state is not anticipated to be well described by a single reference function, the leading coefficients for the strongly closed-shell 1^1A and 3^1A states are quite small (0.808 and 0.763 respectively). Overall, the leading determinants for Nb(III)−salen in Table 13 reveal a much stronger multireference character than

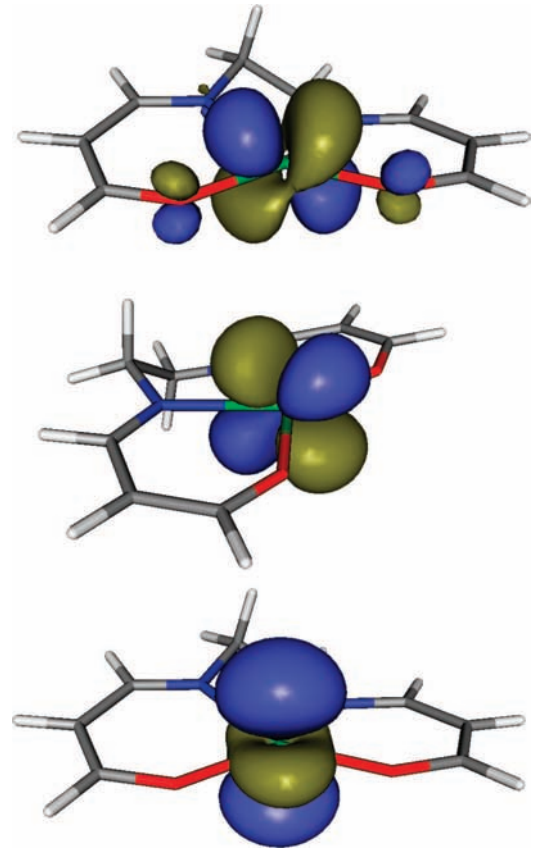

Figure 12. Isosurface plots of the d_{z^2} (lower), d_{xz} (center), and d_{yz} (upper) CASSCF orbitals that comprise the active space for Nb(III)−salen.

those for the iso-electronic Zr(II)−salen presented in Table 11. The BP86 and BPW91 values for the gap between the lowest singlet and triplet states are in reasonable agreement with the CASPT3 results, whereas B3LYP greatly underestimates this energy difference (1.4 vs 19.8 kcal mol^{-1}). Due to the strong nondynamical correlation effects in Nb(III)−salen, the agreement between BP86/BPW91 and CASPT3 appears to be fortuitous. Although we do not report multireference results for the 1^5A state, the DFT results are in agreement that it is much higher in energy (∼50 kcal mol^{-1}) than the low-lying singlets and triplets considered.

The optimized geometries for the 1^1A and 1^3A states of Nb(III)−salen are overlaid in Figure 13 and the LRMSD values are tabulated in Table 5. As can be easily observed either by comparing the geometries for Zr(II)−salen in Figure 10 to those in Figure 12 here or by comparing the LRMSD values from Table 2 to those from Table 5, the overall agreement in the molecular geometries is significantly worse for Nb(III)−salen than for Zr(II)−salen. The maximum LRMSD [0.147 Å in the case of Zr(II)−salen] is now 0.457 Å. The geometries from BP86 and BPW91 are nearly identical, being very close (LRMSD < Å) to the CASSCF geometry for the 1^3A state. However, none of the functionals employed provide reasonable agreement with the CASSCF geometry for the highly multireference 1^1A state. Although the B3LYP 1^1A geometry is closest to that from CASSCF, the LRMSD of 0.326 Å remains quite large. All of the functionals predict the 1^1A state to possess a significant out-of-plane distortion relative to the CASSCF geometry.

Mo(IV)−Salen. The relative energies from all methods for Mo(IV)−salen are included in Table 14, being qualitatively

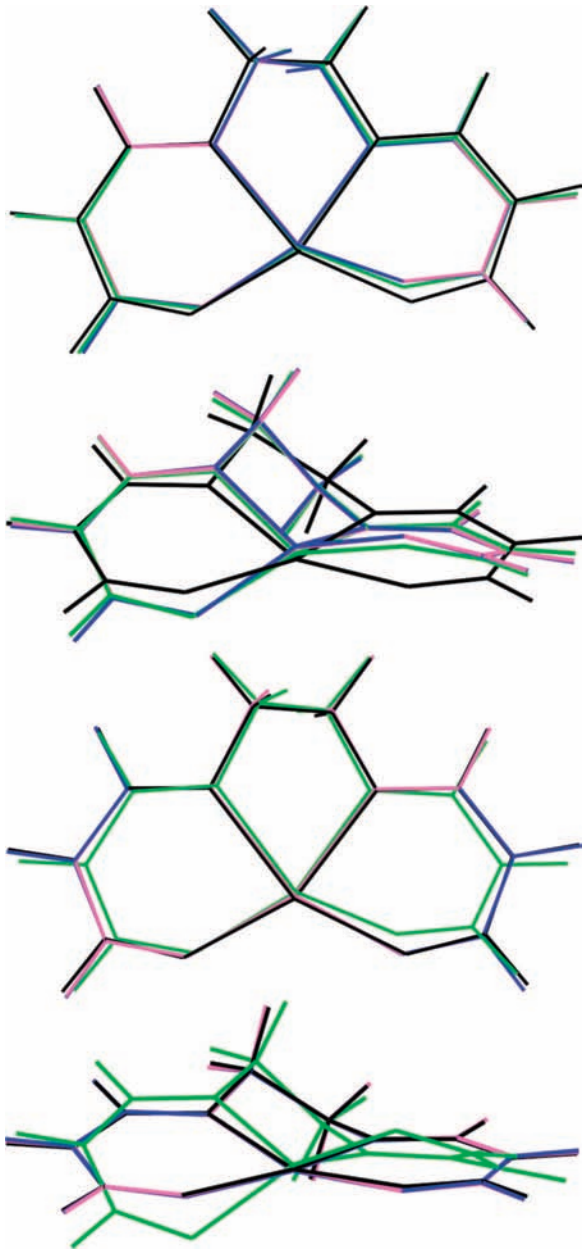

Figure 13. Overlay of the optimized geometries for the 1^1A (top) and 1^3A (bottom) states of Nb(III)−salen from different levels of theory. The theoretical methods include CASSCF (black), B3LYP (green), BP86 (blue), and BPW91 (mauve).

similar to those of the iso-electronic Zr(II)− and Nb(III)−salens presented above. All of the density functionals provide very similar descriptions of the electronic state ordering. Although all functionals place the 1^5A state much lower in energy than that observed in Zr(II)− and Nb(III)−salen, the DFT approaches along with large CAS-CI computations predict the 1^5A state to be fairly well separated from the low-lying singlet and triplet states. The lowest singlet and triplet states are all seemingly well described by the same three-in-two active-space (see Figure 14) employed for the previous systems, and the SA-CASSCF(2/3)/6-31G*[1^1A,2^1A,3^1A,1^3A,2^3A,3^3A] relative energies are included in Table 14. Dynamical correlation corrections are small except for the 2^3A state. The 1^3A−1^1A splitting predicted at the SA-CASSCF level is slightly larger than that observed in Nb(III)−salen or than that predicted by DFT. Unsurprisingly, the B3LYP functional predicts a slightly larger splitting than the BP86 and BPW91 approaches.

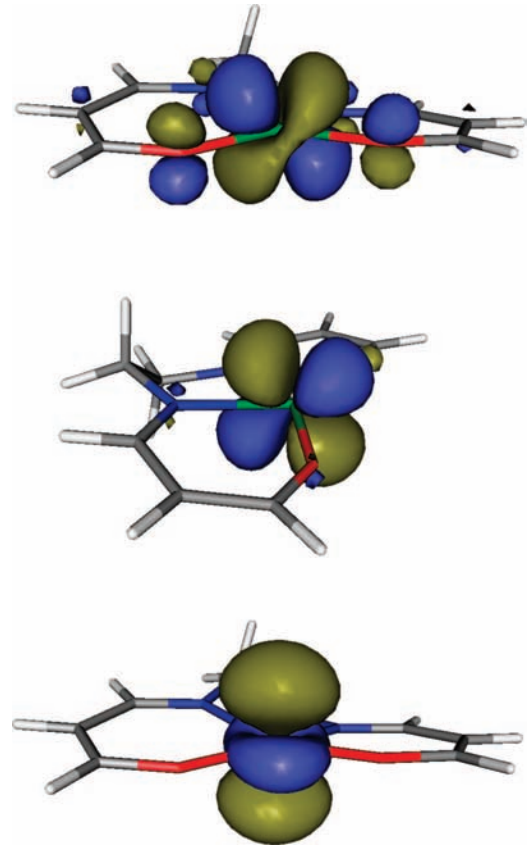

Figure 14. Isosurface plots of the d_{z^2} (lower), d_{xz} (center), and d_{yz} (upper) CASSCF orbitals that comprise the active space for Mo(IV)−salen.

The leading determinants from the SA-CASSCF computations are presented in Table 15 for the lowest singlet and triplet states. Just as in Zr(II)− and Nb(III)−salen, the singlet states appear highly multireference and the triplet states are all strongly single-reference. The 1^1A state becomes increasingly multireference moving from Zr(II)−salen to Mo(IV)−salen. The weight of the leading $(d_{z^2})^2$ determinant becomes increasingly smaller [being 0.909, 0.808, 0.762 for Zr(II)−, Nb(III)−, and Mo(IV)−salen, respectively]. At the same time, the substantial weight of the $(d_{xz})^2$ configuration becomes increasingly larger [being −0.408, −0.586, and −0.646 for the same systems].

The optimized geometries for the 1^1A and 1^3A states of Mo(IV)−salen from the various levels of theory are depicted in Figure 15 and the computed LRMSD values are presented in Table 9. The CASSCF molecular geometries (especially for the 1^1A state) are noticeably more planar than those from the DFT approaches. As can be observed from the LRMSD values in Table 9, the BP86 and BPW91 geometries are nearly identical and are very similar to those provided by the B3LYP functional. All of the DFT approaches provide geometries that are significantly different from the CASSCF geometries, although less so for the 1^3A state than for the 1^1A state.

Conclusions

The results presented here clearly establish strong nondynamical correlation effects in the d^2-metal salen systems. With the exception of Cr(IV)−salen, all of the systems examined were found to posses a 1^3A ground state. The 1^1A states were observed to lie 10−30 kcal mol^{-1} higher in energy, with the singlet−triplet splitting increasing with increasing formal oxidation state at the metal center. The 1^1A states were observed to

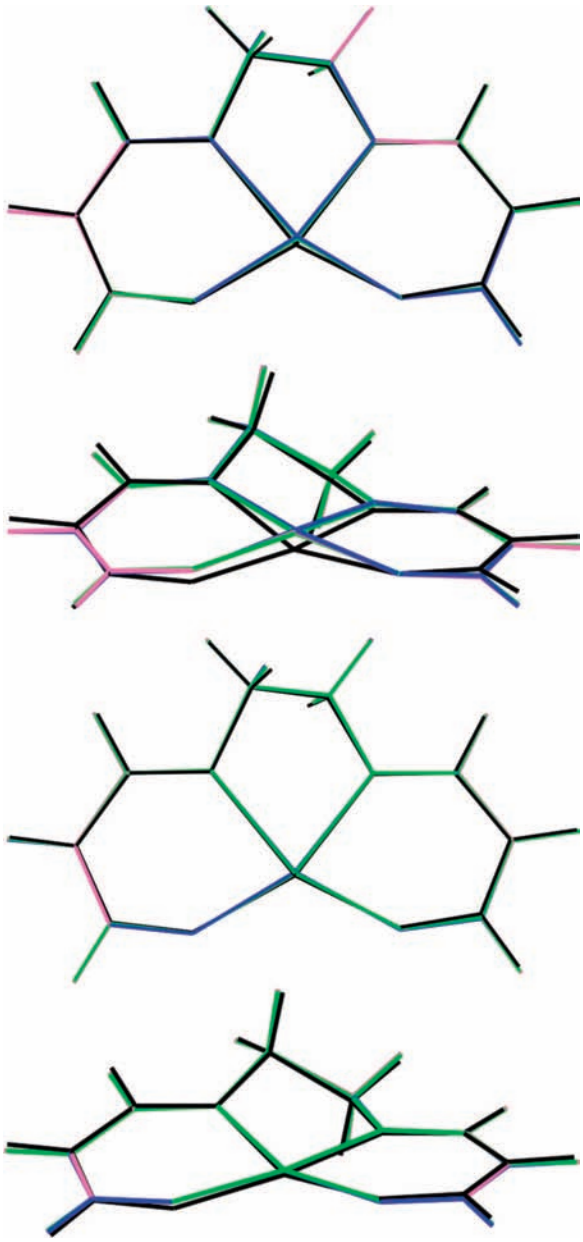

Figure 15. Overlay of the optimized geometries for the 1^1A (top) and 1^3A (bottom) states of Mo(IV)−salen from different levels of theory. The theoretical methods include CASSCF (black), B3LYP (green), BP86 (blue), and BPW91 (mauve).

become increasingly multireference with the increasing oxidation state (based upon both decreasing C_0 and increasing C_1 coefficients), in contrast to the 1^3A states becoming increasingly single-reference. With the exception of Cr(IV)−salen, all of the systems were well described by a relatively small 2-in-3 active space. Interestingly, the 4d metal−salens exhibit similar non-dynaical correlation effects as the corresponding 3d system. The leading coefficients from the SA-CASSCF computations are similar in each.

The results from three commonly-employed density functionals were benchmarked against those from CASSCF and CASPT3. Given the strong multireference character of many of the states examined, the generally reasonable performance of DFT is surprising. With the exception of the Nb(III)−salen system, all three functionals provide geometries that are typically within 0.2 Å LRMSD of the corresponding CASSCF geometry. The performance for relative energies was observed to be somewhat worse, with B3LYP providing relative energies closer to the CASPT3 results than BP86 or BPW91 for all systems studied except Nb(III)−salen. As has been observed in our previous work, the choice of the exchange functional remains the central concern when selecting an appropriate DFT approach for metal−ligand systems such as these. The results from BP86 and BPW91 are nearly identical for all systems. With the exception of Nb(III)−salen, B3LYP was found to provide relative energies superior to those from BP86 or BPW91. Both the BP86 and BPW91 approaches tend to underestimate the relative stability of the high-spin 1^3A states. Although none of the functionals employed provided reliable results for Nb(III)−salen, B3LYP was observed to provide geometries and relative energies closer to our benchmark values for the remainder of the systems examined.

Acknowledgment. We thank the U.S. Department of Energy, Basic Energy Sciences, for financial support of this work through Catalysis Science Grant/Contract No. DE-FG02-03ER15459. The Center for Computational Molecular Science and Technology is funded through a Shared University Research (SUR) grant from IBM, by a CRIF grant from NSF (CHE-0443564), and by Georgia Tech.

Supporting Information Available: The coordinates for all states from the SA-CASSCF optimized geometries are included in the supporting information.This material is available free of charge via the Internet at http://pubs.acs.org.

References and Notes

(1) Venkataramanan, N. S.; Kuppuraj, G.; Rajagopal, S. *Coord. Chem. Rev.* **2005**, *249*, 1249.
(2) McGarrigle, E. M.; Gilheany, D. G. *Chem. Rev.* **2005**, *105*, 1563.
(3) Canali, L.; Sherrington, D. C. *Chem. Soc. Rev.* **1999**, *28*, 85.
(4) Zheng, X. L.; Jones, C. W.; Weck, M. *Chem. Eur. J.* **2005**, *12*, 576.
(5) Strassner, T.; Houk, K. N. *Org. Lett.* **1999**, *1*, 419.
(6) Khavrutskii, I. V.; Musaev, D. G.; Morokuma, K. *Proc. Natl. Acad. Sci. U.S.A.* **2004**, *101*, 5743.
(7) Jacobsen, H.; Cavallo, L. *Phys. Chem. Chem. Phys.* **2004**, *6*, 3747.
(8) Ivanic, J.; Collins, J. R.; Burt, S. K. *J. Phys. Chem. A* **2004**, *108*, 2314.
(9) Ivanic, J. *J. Chem. Phys.* **2003**, *119*, 9377.
(10) Abashkin, Y. G.; Collins, J. R.; Burt, S. K. *Inorg. Chem.* **2001**, *40*, 4040.
(11) Khavrutskii, I. V.; Musaev, D. G.; Morokuma, K. *Inorg. Chem.* **2005**, *44*, 306.
(12) Khavrutskii, I. V.; Rahim, R. R.; Musaev, D. G.; Morokuma, K. *J. Phys. Chem. B* **2004**, *108*, 3845.
(13) Khavrutskii, I. V.; Musaev, D. G.; Morokuma, K. *J. Am. Chem. Soc.* **2003**, *125*, 13879.
(14) Linde, C.; Arnold, M.; Norrby, P. O.; Akermark, B. *Angew. Chem. Int. Ed.* **1997**, *36*, 1723.
(15) Linde, C.; Akermark, B.; Norrby, P. O.; Svensson, M. *J. Am. Chem. Soc.* **1999**, *121*, 5083.
(16) Jacobsen, H.; Cavallo, L. *Chem. Eur. J.* **2001**, *7*, 800.
(17) Cavallo, L.; Jacobsen, H. *Inorg. Chem.* **2004**, *43*, 2175.
(18) Cavallo, L.; Jacobsen, H. *J. Phys. Chem. A* **2003**, *107*, 5466.
(19) Cavallo, L.; Jacobsen, H. *J. Org. Chem.* **2003**, *68*, 6202.
(20) Cavallo, L.; Jacobsen, H. *Angew. Chem. Int. Ed.* **2000**, *39*, 589.
(21) Abashkin, Y. G.; Burt, S. K. *Org. Lett.* **2004**, *6*, 59.
(22) Sears, J. S.; Sherrill, C. D. *J. Chem. Phys.* **2006**, *124*, 144314.
(23) Sears, J. S.; Sherrill, C. D. *J. Phys. Chem. A* **2008**, *112*3466.
(24) Davidson, E. R. *Chem. Rev.* **1991**, *91*, 649.
(25) Kohn, W.; Sham, L. J. *Phys. Rev.* **1965**, *140*, 1133.
(26) Hohenberg, P.; Kohn, W. *Phys. Rev. B* **1964**, *136*, B864.
(27) Chermette, H. *Coord. Chem. Rev.* **1998**, *180*, 699.
(28) Holthausen, M. C. *J. Comp. Chem.* **2005**, *26*, 1505.
(29) Yanagisawa, S.; Tsuneda, T.; Hirao, K. *J. Chem. Phys.* **2000**, *112*, 545.
(30) Barden, C. J.; Rienstra-Kiracofe, J. C.; Schaefer, H. F. *J. Chem. Phys.* **2000**, *113*, 690.
(31) Nakao, Y.; Hirao, K.; Taketsugu, T. *J. Chem. Phys.* **2001**, *114*, 7935.

(32) Harrison, J. F. *Chem. Rev.* **2000**, *100*, 679.
(33) Zhao, Y.; Truhlar, D. G. *J. Chem. Phys.* **2006**, 124.
(34) Quintal, M. M.; Karton, A.; Iron, M. A.; Boese, A. D.; Martin, J. M. L. *J. Phys. Chem. A* **2006**, *110*, 709.
(35) Wang, S. G.; Schwarz, W. H. E. *J. Chem. Phys.* **1998**, *109*, 7252.
(36) Wodrich, M. D.; Corminboeuf, C.; Schleyer, P. V. *Org. Lett.* **2006**, *8*, 3631.
(37) Schmidt, M. W.; Gordon, M. S. *Ann. Rev. Phys. Chem.* **1998**, *49*, 233.
(38) Roos, B. O.; Taylor, P. R. *Chem. Phys.* **1980**, *48*, 157.
(39) Sherrill, C. D.; Schaefer, H. F. *Adv. Quantum Chem.* **1999**, *34*, 143.
(40) Rulisek, L.; Havlas, Z. *Int. J. Quantum Chem.* **2003**, *91*, 504.
(41) Bernardi, F.; Bottoni, A.; Garavelli, M. *Quant. Struct.-Act. Relat.* **2002**, *21*, 128.
(42) Glukhovtsev, M. N.; Bach, R. D.; Nagel, C. J. *J. Phys. Chem. A* **1997**, *101*, 316.
(43) Roos, B. O.; Andersson, K.; Fulscher, M. P.; Malmqvist, P. A.; SerranoAndres, L.; Pierloot, K.; Merchan, M. *In Advances in Chemical Physics Vol Xciii* **1996**, *93*, p 219.
(44) Vallet, V.; Bossert, J.; Strich, A.; Daniel, C. *Phys. Chem. Chem. Phys.* **2003**, *5*, 2948.
(45) Meier, R. J. *Comp. Mat. Sci.* **2003**, *27*, 219.
(46) Cai, Z. L.; Sendt, K.; Reimers, J. R. *J. Chem. Phys.* **2002**, *117*, 5543.
(47) Franceschi, F.; Solari, E.; Floriani, C.; Rosi, M.; Chiesi-Villa, A.; Rizzoli, C. *Chem. Eur. J.* **1999**, *5*, 708.
(48) Liu, Z. H.; Anson, F. C. *Inorg. Chem.* **2001**, *40*, 1329.
(49) Liu, Z. H.; Anson, F. C. *Inorg. Chem.* **2000**, *39*, 274.
(50) Yamamoto, K.; Oyaizu, K.; Tsuchida, E. *J. Am. Chem. Soc.* **1996**, *118*, 12665.
(51) Bakac, A.; Guzei, I. A. *Inorg. Chem.* **2000**, *39*, 736.
(52) Watanabe, A.; Uchida, T.; Irie, R.; Katsuki, T. *Proc. Natl. Acad. Sci. U.S.A.* **2004**, *101*, 5737.
(53) Watanabe, A.; Uchida, T.; Ito, K.; Katsuki, T. *Tetrahedron Lett.* **2002**, *43*, 4481.
(54) Miyazaki, T.; Katsuki, T. *Synlett* **2003**, 1046.
(55) Luts, T.; Suprun, W.; Hofmann, D.; Klepel, O.; Papp, H. *J. Mol. Cat. A* **2007**, *261*, 16.
(56) Jaguar 5.5; Schrödinger, L.L.C.: Portland, OR, 1991-2003.
(57) Becke, A. D. *Phys. Rev. A* **1988**, *38*, 3098.
(58) Perdew, J. P. *Phys. Rev. B* **1986**, *33*, 8822.
(59) Perdew, J. P.; Wang, Y. *Phys. Rev. B* **1992**, *45*, 13244.
(60) Becke, A. D. *J. Chem. Phys.* **1993**, *98*, 5648.
(61) Lee, C. T.; Yang, W. T.; Parr, R. G. *Phys. Rev. B* **1988**, *37*, 785.
(62) Chasman, D.; Beachy, M. D.; Wang, L. M.; Friesner, R. A. *J. Comp. Chem.* **1998**, *19*, 1017.
(63) Hay, P. J.; Wadt, W. R. *J. Chem. Phys.* **1985**, *82*, 270.
(64) Francl, M. M.; Pietro, W. J.; Hehre, W. J.; Binkley, J. S.; Gordon, M. S.; Defrees, D. J.; Pople, J. A. *J. Chem. Phys.* **1982**, *77*, 3654.
(65) Werner, H. J.; Knowles, P. J.; Lindh, R.; Manby, F. R.; Schütz, M.; Celani, P.; Korona, T.; Rauhut, G.; Amos, R. D.; Bernhardsson, A.; Berning, A.; Cooper, D. L.; Deegan, M. J. O.; Dobbyn, A. J.; Eckert, F.; Hampel, C.; Hetzer, G.; Lloyd, A. W.; McNicholas, S. J.; Meyer, W.; Mura, M. E.; Nicklass, A.; Palmieri, P.; Pitzer, R.; Schumann, U.; Stoll, H.; Stone, A. J.; Trarroni, R.; Thorsteinsson, T.;MOLPRO 2006.1.
(66) Pietro, W. J.; Hehre, W. J. *J. Comp. Chem.* **1983**, *4*, 241.
(67) Hehre, W. J.; Ditchfie, R.; Stewart, R. F.; Pople, J. A. *J. Chem. Phys.* **1970**, *52*, 2769.
(68) Hehre, W. J.; Stewart, R. F.; Pople, J. A. *J. Chem. Phys.* **1969**, *51*, 2657.
(69) Humphrey, W.; Dalke, A.; Schulten, K. *J. Mol. Graphics Modell.* **1996**, *14*, 33.
(70) Portmann, S.; Luthi, H. P. *Chimia* **2000**, *54*, 766.
(71) Wissing, K.; Degen, J. *THEOCHEM* **1998**, *431*, 97.
(72) Messmer, R. P.; Interran, Lv.; Johnson, K. H. *J. Am. Chem. Soc.* **1974**, *96*, 3847.
(73) Rosch, N.; Messmer, R. P.; Johnson, K. H. *J. Am. Chem. Soc.* **1974**, *96*, 3855.
(74) Edmiston, C.; Ruedenberg, K. *Rev. Mod. Phys.* **1963**, *35*, 457.
(75) Siegbahn, P. E. M. *Adv. Chem. Phys.* **1996**, *XCIII*, 333.

JP802249N